Environmental Science & Technology

Article

Cite This: Environ. Sci. Technol. 2018, 52, 11642−11651

pubs.acs.org/est

Reactive Oxygen Species Formed by Secondary Organic Aerosols in Water and Surrogate Lung Fluid

Haijie Tong,*[,†] Pascale S. J. Lakey,[†,‡] Andrea M. Arangio,[†] Joanna Socorro,[†] Fangxia Shen,[†] Kurt Lucas,[†] William H. Brune,[§] Ulrich Pöschl,[†] and Manabu Shiraiwa*[,†,‡]

[†]Multiphase Chemistry Department, Max Planck Institute for Chemistry, 55128 Mainz, Germany

[‡]Department of Chemistry, University of California, Irvine, California 92697-2025, United States

[§]Department of Meteorology, Pennsylvania State University, University Park, Pennsylvania 16802, United States

Supporting Information

ABSTRACT: Reactive oxygen species (ROS) play a central role in adverse health effects of air pollutants. Respiratory deposition of fine air particulate matter can lead to the formation of ROS in epithelial lining fluid, potentially causing oxidative stress and inflammation. Secondary organic aerosols (SOA) account for a large fraction of fine particulate matter, but their role in adverse health effects is unclear. Here, we quantify and compare the ROS yields and oxidative potential of isoprene, β-pinene, and naphthalene SOA in water and surrogate lung fluid (SLF). In pure water, isoprene and β-pinene SOA were found to produce mainly OH and organic radicals, whereas naphthalene SOA produced mainly H_2O_2 and $O_2^{\bullet-}$. The total molar yields of ROS of isoprene and β-pinene SOA were 11.8% and 8.2% in water and decreased to 8.5% and 5.2% in SLF, which can be attributed to ROS removal by lung antioxidants. A positive correlation between the total peroxide concentration and ROS yield suggests that organic (hydro)peroxides may play an important role in ROS formation from biogenic SOA. The total molar ROS yields of naphthalene SOA was 1.7% in water and increased to 11.3% in SLF. This strong increase is likely due to redox reaction cycles involving environmentally persistent free radicals (EPFR) or semiquinones, antioxidants, and oxygen, which may promote the formation of H_2O_2 and the adverse health effects of anthropogenic SOA from aromatic precursors.

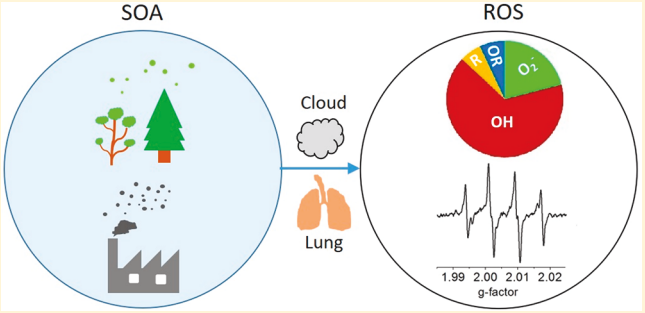

INTRODUCTION

Secondary organic aerosols (SOA) are a major component of tropospheric aerosols, affecting climate, air quality, and public health. SOA are formed through the oxidation of biogenic and anthropogenic volatile organic compounds, followed by the nucleation or partitioning of semivolatile, low-volatile, or extremely low-volatile organic products from the gas phase to the particle phase.[1] Particle-phase chemistry and cloud processing are also efficient SOA formation pathways.[2] Despite recent progress in the understanding of the molecular composition of SOA,[3] their role in adverse aerosol health effects is still largely unknown.[4]

Reactive oxygen species (ROS) play a central role in physiological processes by mediating metabolism and causing oxidative stress.[5] ROS, which are mostly formed by the reduction of oxygen, include singlet oxygen, OH radicals, superoxide radicals ($O_2^{\bullet-}$), organic radicals, and hydrogen peroxide (H_2O_2).[4,6] It has been shown that ROS can be formed by particulate matter containing redox-active components such as transition metals and humic-like substances.[7−9] Particle-bound ROS can be detected using techniques such as electron paramagnetic resonance (EPR) spectroscopy,[10−12] mass spectrometry, and fluorescence probes.[13] In addition, assays based on dithiothreitol (DTT),[14] macrophage cells,[15] and ascorbate,[16] as well as online microfluidic electrochemical sensors[17] have been used to evaluate the oxidative potential and redox activity of atmospheric aerosols. The DTT assay has been used widely to evaluate the oxidative potential of transition metals,[14] quinones,[8,14,18] organic peroxides,[19] and SOA.[20] Furthermore, it has also been found that oxidative potential of atmospheric particulate matter depends on their sizes,[21] compositions,[22] emission sources,[23] and formation and aging processes.[24,25] Finally, oxidative potential has also been linked to oxidative stress and asthma caused by atmospheric particle matter.[21,26,27] Despite recent progress, the connections between ROS formation yields and redox activity of atmospheric particulate matter are not yet fully established.[28]

Recent studies have shown that decomposition of organic hydroperoxides in SOA can lead to the formation of OH radicals in the aqueous phase under dark[10,29] and irradiated conditions.[30] Atmospheric fine particles contain environmentally

Received: July 5, 2018
Revised: September 5, 2018
Accepted: September 20, 2018
Published: September 20, 2018

DOI: 10.1021/acs.est.8b03695
Environ. Sci. Technol. 2018, 52, 11642−11651

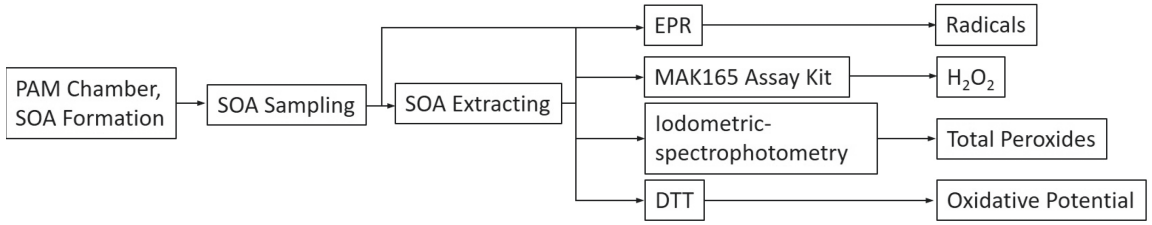

Figure 1. Schematic outline of the experimental approach: generation and sampling of SOA, SOA extraction by water or SLF, and application of different experimental techniques to measure radicals, H_2O_2, peroxides, and oxidative potential.

persistent free radicals (EPFR) such as semiquinone radicals, which can be formed via combustion or pyrolysis of organic matter[31−33] as well as heterogeneous reactions of ozone with polycyclic aromatic hydrocarbons.[34,35] EPFR can undergo redox-active reactions generating ROS, which may contribute to cellular oxidative stress and cytotoxicity.[12,36] Therefore, the detection and quantification of different ROS species is required for better understanding of SOA health effects. In this study, we applied EPR spectroscopy in combination with a spin-trapping technique and DTT assay to investigate reactions of SOA components in liquid water or surrogate lung fluid, quantifying the total ROS yield as well as the yield of each radical species formed by SOA. A kinetic model was applied for data analysis and interpretation to better understand the ROS formation mechanism by different types of SOA.[36]

EXPERIMENTAL SECTION

SOA Formation, Characterization, and Collection. A schematic drawing on the experimental procedure used in this study is shown in Figure 1. SOA were produced in a 19 L potential aerosol mass (PAM) chamber through ozonolysis of β-pinene or gas phase photooxidation of isoprene and naphthalene with OH radicals.[37] Briefly, 2−3 mL of isoprene (99%, Sigma-Aldrich) were placed in an amber glass vial, and a ∼500 μm hole was drilled into its cap to enable precursor evaporation. The vial containing the isoprene liquid was kept in another 250 mL Duran bottle. A 1 bar and 250 ccm N_2 (99.999%, Westfalen AG) flow was passed through the Duran bottle and carried the gas phase isoprene into the PAM chamber for SOA formation via photochemical oxidation with OH radicals. β-Pinene (99%, Sigma-Aldrich) was placed in a 1.5 mL amber glass vial (VWR International GmbH), and 5−10 g of naphthalene crystals (99.6%, Alfa Aesar GmbH & Co KG) were put in a 100 mL glass bottle (DURAN Group GmbH) as SOA precursor sources. Flows of 1 bar and 50−150 ccm N_2 (99.999%, Westfalen AG) were used as a carrier gas to introduce β-pinene and naphthalene vapors into the 19 L PAM chamber for a reaction with oxidants (O_3 or OH radicals) for ∼5 min. Ozone concentrations in the PAM chamber were ∼1 ± 0.2 ppm for naphthalene SOA formation and 10 ± 5 ppm for isoprene and β-pinene SOA formation, as measured with an ozone monitor (model 49i, Thermo Fisher Scientific Inc.). The relative humidity was 0−5% for β-pinene SOA and 30−40% for formation of isoprene and naphthalene SOA to have higher OH concentrations in the chamber. On the basis of the exposure estimation equations by Peng et al.,[38] the gas phase OH radical concentrations are estimated to be $\sim 5 \times 10^{11}$ cm^{-3}, which is much higher than ambient concentrations. It is worth noting that SOA generated by the PAM chamber have been shown to be a good surrogate for chamber-generated SOA in terms of their oxidation state, chemical composition, and hygroscopicity.[39,40] For EPR and other supporting analysis, a substantial amount of SOA mass (about 0.1−5 mg) is necessary, and the PAM chamber is a robust instrument to generate such high mass in relatively short time. Nevertheless, relevance and limitations of PAM-generated SOA need to be investigated and SOA formed in ambient-relevant conditions would need to be tested in future studies.

SOA was collected on 47 mm Omnipore Teflon filters (100 nm pore size, Merck Chemicals GmbH). The sampling time varied from several minutes to several hours depending on the required aerosol mass. Filtered SOA particles were normally analyzed immediately. A scanning mobility particle sizer (SMPS, GRIMM Aerosol Technik GmbH & Co. KG) was used to characterize the size and mass concentrations of the generated SOA particles. The typical size of the SOA ranged from 50 to 600 nm, and the typical mass concentration range was from 100 to 1500 μg m^{-3} (a density of 1.4 g cm^{-3} was used[1]). A flow rate of ∼3 L min^{-1} was controlled using a common diaphragm vacuum pump (0−3 L min^{-1}), which was connected after the aerosol samplers. Blank tests confirmed that blank filters produced no radicals, and the condensation of water vapor on a filter during SOA collection was negligible for the relative humidities applied in this study. SOA particles on Teflon filters were extracted into a 1 mL water solution containing spin trapping agents (10 mM) with a vortex shaker (Heidolph Reax 1) for 10 min at 2500 rpm. Each of the glass vials (VWR International GmbH) was rinsed for 5−10 times with 5 mL fresh Milli-Q water and dried under ultrapure dry nitrogen gas (99.999%, Westfalen AG) before SOA extraction. Measurements with water blanks confirmed little anthropogenic interferences such as laboratory dust contamination.[10] Vials were used only once to avoid contamination from residues. The final SOA concentration depends on the aerosol mass load and extraction time. An average molar mass of 200 g mol^{-1} for SOA was used for calculating SOA concentrations. The pH of SOA solutions here was in the range of 3.5−6.5 (Figure S4).

SOA extracts were mixed with surrogate lung fluid (SLF),[7] which contain 114 mM NaCl, 10 mM phosphate-buffered saline (2.2 mM KH_2PO_4 and 7.8 mM Na_2HPO_4), 200 μM ascorbic acid sodium salt, 300 μM citric acid, 100 μM reduced L-glutathione, and 100 μM uric acid sodium salt.

CW-EPR Measurement. A continuous wave electron paramagnetic resonance (CW-EPR) spectrometer (EMXplus-10/12, Bruker, Germany) was applied for detecting radicals. The parameter set for EPR measurements in this study was a modulation frequency of 100 kHz, a microwave frequency of 9.84 GHz, a microwave power of 2.15 mW (20 db), a modulation amplitude of 1.0 G, a sweep width of 60.0 G, a sweep time of 10.49 s, a receiver gain of 40 db, a time constant of 0.32 ms, a conversion time of 10.24 ms, and a scan number of 10−50 (Figure 2). A spin trapping technique was applied by mixing particle extracts with 5-tert-butoxycarbonyl-5-methyl-1-pyrroline-*N*-oxide (BMPO, high purity, Enzo Life Sciences

DOI: 10.1021/acs.est.8b03695
Environ. Sci. Technol. 2018, 52, 11642−11651

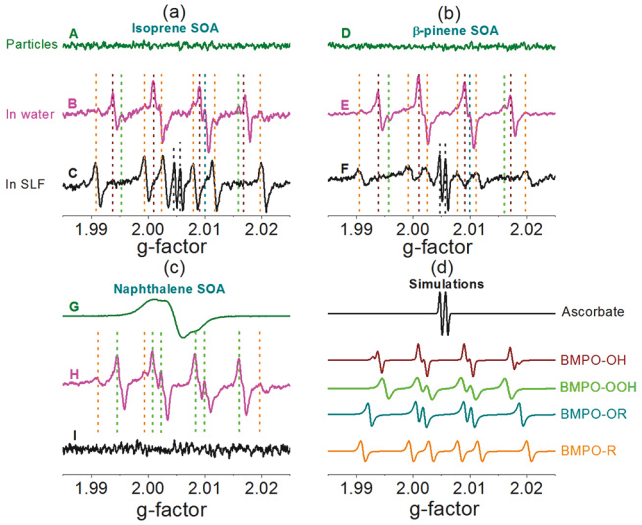

Figure 2. EPR spectra of radicals in SOA from (a) isoprene, (b) β-pinene, and (c) naphthalene as collected on filters (EPFR, dark green lines) and after extraction with water (pink lines) and surrogate lung fluid (black line). (d) Simulations of EPR spectra for ascorbate radicals, BMPO-OH, BMPO-OOH, BMPO-OR, and BMPO-R adducts. The dashed vertical lines in (a–c) indicate different radical species referring to the simulated spectra in (d) and their color code.

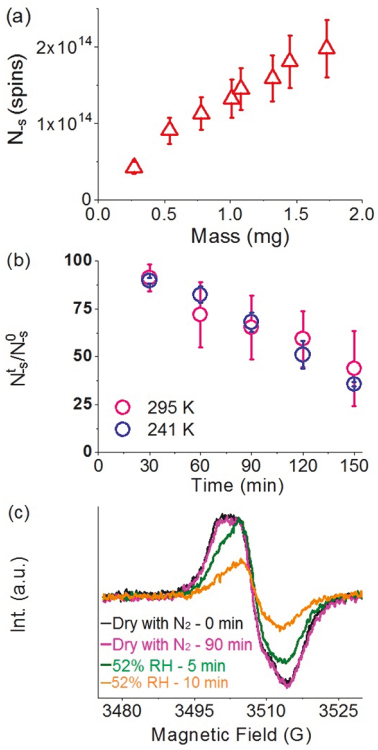

Figure 3. Concentrations and lifetime of EPFR associated with naphthalene SOA. (a) Number of spins (N_S) vs mass of naphthalene SOA in investigated filter samples). (b) Decay rate of EPFR at 295 and 241 K. N^0_S: number of spins in naphthalene SOA at time 0. N^t_S: number of spins in naphthalene SOA at time *t*. (c) The EPR spectra of naphthalene SOA under dry and humid conditions. Error bars in (a) are radical concentration uncertainty based on calibration curves. Error bars in (b) are one standard deviation based on 3 replicates.

GmbH). BMPO reacts with radical types of ROS (e.g., OH, $O_2^{\bullet-}$, organic radicals) to form stable radical adducts that can be detected by EPR, so that concentrations of different radical-adducts can be quantified. The relative yields of each adduct were obtained using the Matlab-based computational package Easyspin.[41] In addition, a spin probing technique with the use of 1-hydroxy-2,2,6,6-tetramethyl-4-oxo-piperidine (TEMPONE-H, Enzo Life Sciences GmbH) was applied to quantify total concentrations of radical types of ROS. In contrast to the adducting mechanism of BMPO,[42] TEMPONE-H (which is a closed-shell molecule) can be converted to radicals via deprotonation by reacting with radicals.[43] It has been found that TEMPONE-H has significantly higher sensitivity in the detection of superoxide radicals than BMPO with reported rate coefficients of 1.2×10^4 M^{-1} s^{-1} for TEMPONE-H[43] and 77 M^{-1} s^{-1} for BMPO.[44] Therefore, we speculate that the sensitivity of TEMPONE-H and BMPO for detecting organic radicals may also be different. Thus, BMPO was used to distinguish different types of radicals, while TEMPONE-H has a higher radical detection efficiency relative to BMPO and was used to quantify the total radicals (OH, $O_2^{\bullet-}$, organic radicals).

A spin counting method[45] was applied for radical quantification. This method is based on double integration allowing the peak area of a spectrum to be obtained.[46] The area is positively correlated with the radical concentrations. A calibration curve for the stable radical TEMPOL enabled the exact radical concentration of SOA extracts to be obtained.[10] The calibration curve also confirmed the reliability of the spin counting method.[10,11] The error bars in Figure 3 (panels a and b), Figure 4 (panels a and b), and Figure 6 included the uncertainties in the SOA mass measurements and the estimated deviations from the TEMPOL calibration curve.

Superoxide dismutase (SOD) enzymes were used to confirm the existence of $HO_2/O_2^{\bullet-}$ (Figure S3). The black spectrum in Figure S3 is for the BMPO adducts in isoprene SOA water extracts. The green dashed line highlights the typical signal of $HO_2/O_2^{\bullet-}$. When the SOD was present, the typical peaks of $HO_2/O_2^{\bullet-}$ diminished significantly, indicating that SOD scavenged $HO_2/O_2^{\bullet-}$ effectively. This also confirmed the formation of $HO_2/O_2^{\bullet-}$ in isoprene SOA water extracts.

LC–MS/MS. The solutions were analyzed using a 1260 Infinity Bioinert Quaternary LC system with a quaternary pump (G5611A), a HiP sampler (G5667A), and an electrospray ionization (ESI) source interfaced to a Q-TOF mass spectrometer (6540 UHD Accurate-Mass Q-TOF, Agilent). MassHunter software (B.06.01, Agilent) controlled all modules. The LC column was a Zorbax Extend-C18 Rapid resolution HT (2.1 × 50 mm, 1.8 μm) with a column temperature at 30 °C. The mobile phases used were 3% (v/v) acetonitrile (HPLC Gradient grade, Fisher Chemical) in water with formic acid (0.1% v/v, LC–MS Chromasolv, Sigma-Aldrich) (eluent A) and 3% water in acetonitrile (eluent B). The injection volume was 95 μL. The flow rate was 0.2 mL min^{-1} with a gradient program that started with 3% B for 3 min followed by a 36 min step that raised eluent B to 60%. Further, eluent B was increased to 80% at 40 min and returned to the initial conditions within 0.1 min, followed by column re-equilibration for 9.9 min before the next run.

The ESI-Q-TOF instrument was operated in the positive ionization mode (ESI+) with a 325 °C gas temperature, 20 psig nebulizer, 4000 V capillary voltage, and 90 V fragmentor voltage. During the full spectrum MS mode, no collision energy was used to collect species as their molecular ions. During MS/MS analysis that was employed for the structure determination, the fragmentation of protonated ions was conducted using the

DOI: 10.1021/acs.est.8b03695
Environ. Sci. Technol. 2018, 52, 11642–11651

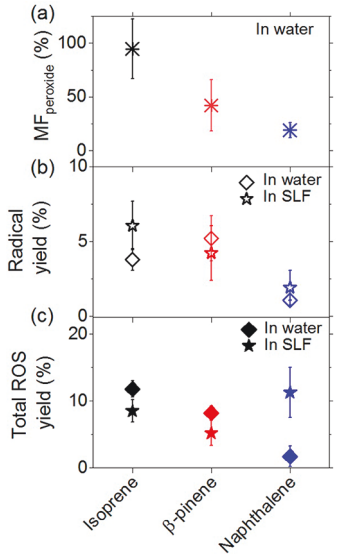

Figure 4. (a) Peroxide mass fraction, (b) yields of total radicals in water and SLF, and (c) yields of H_2O_2 and total radicals in water and SLF of isoprene, β-pinene, and naphthalene SOA. The concentrations of peroxides in (a) were measured using iodometric-spectroscopy. The radical yields were measured using TEMPONE-H as a spin probe. All the error bars are 1 δ standard deviation based on more than 3 replicates. The initial concentration of SOA in water and SLF extract is 1 mM. More details about the iodometric-spectroscopy method, composition of SLF, and extraction methods were given in the Experimental Section and Supporting Information.

target MS/MS mode with a 10 V collision energy. Spectra were recorded over the mass range of m/z 70−500. Data analysis was performed using qualitative data analysis software (B.06.00, Agilent).

Blank solutions were also prepared with three blank filters, and background signals were subtracted on the spectrum MS for identification. The radicals trapped by BMPO within different types of SOA are listed in Table S1. LC−MS/MS spectra and a fragmentation mechanism of $[BMPO + C_5H_9O + H]^+$ forming from isoprene SOA, $[BMPO + C_9H_{15}O_2 + H]^+$ from β-pinene SOA, and $[BMPO + OOH + H]^+$ from naphthalene SOA are shown in Figure S1. A C_4H_8 fragment was observed for all of the identified radical adducts, indicating a uniform fragmentation pathway.

DTT Assay. The dithiothreitol (DTT) assay was used to assess the oxidation potential of isoprene, β-pinene, and naphthalene SOA. The details of this method can be found in previous studies.[47,48] Briefly 0.1 mol potassium phosphate monobasic-sodium hydroxide (KH_2PO_4) and 0.4 mol disodium hydrogen phosphate (Na_2HPO_4) were dissolved into 1 L DI water (TraceSELECT Ultra ACS reagent water, Sigma-Aldrich) to form a 0.5 M buffer solution. The 0.5 M buffer solution was diluted 10 times to form a 0.05 M buffer solution (pH = 7.4). A 0.5 M ethylenediaminetetraacetic acid (EDTA) stock solution was made and diluted 500 times with the above 0.05 M buffer, which was used as a working buffer. DTT (>98%, Sigma-Aldrich) was dissolved in 10 mL of the working buffer and diluted to form a 0.5 mM working solution. DTNB was dissolved in working buffer and diluted to form a 1 mM working solution.

A mixture of 1.5 mL working buffer, 75 μL of 0.5 mM DTT, and 300 μL of SOA extract was incubated at 37 °C and measured for 35 min. After 7 min intervals, 300 μL of the mixture was mixed with 16 μL of 1 mM DTNB solution and the mixture's UV absorption at 412 nm was measured. The decay rate of DTT during the incubation process was used to characterize the oxidative potential of SOA. A plate reader (Synergy NEO, BioTek Instruments, Inc.) was used for the absorption measurement. At least 3 replicates were measured for each data point. A calibration curve for DTT is shown in Figure S2a. The absorbance intensity of DTT at 412 nm has a positive and linear relationship with its concentration. The absorbance intensity increased from ∼0.06 to ∼0.52 as the DTT amount increased from 0 to 37.5 nmol. The consumption rate of DTT by 1,2 NQN is around 15181 pmol min^{-1} μg^{-1}, which is consistent with a previous study.[49] The consumption rates of DTT by SOA water extracts are shown in Figure S2b. In water extracts, the naphthalene SOA showed the highest DTT consumption rate of ∼0.51 nM min^{-1}, followed by isoprene and β-pinene SOA with rates of ∼0.11 and ∼0.03 nM min^{-1}.

Total Peroxides and H_2O_2 Quantification. A modified iodometric-spectrophotometric method[50] was used for quantifying the total peroxides in SOA. First, isoprene, β-pinene, and naphthalene SOA were extracted into ethyl acetate, and their concentrations were adjusted to be 0.4 or 0.5 mM. Second, 2 mL of the extract was mixed with 3 mL of an acetic acid-chloroform-water (v:v 0.53:0.27:0.20) solution and purged with a flow of 15 ccm N_2 for 2 min to exclude dissolved oxygen. Third, 50 mg potassium iodide was added into the solution, and the vial was capped and sealed with parafilm immediately. The solution was allowed to stand for 1 h. Finally, 300 μL of this solution was transferred to a 96 well plate and the absorbance at 470 nm was measured with a microplate reader. This absorbance intensity was used to calculate the peroxide abundance in SOA, and a calibration curve for benzoyl peroxide was used as shown in Figure S5. The absorbance intensity of benzoyl peroxide at 470 nm has a linear relationship with its concentration in the range of 0−1 mM.

We used a Fluorimetric Hydrogen Peroxide Assay Kit (MAK165, Sigma) to measure the H_2O_2 yield of SOA. First, aliquots of assay buffer, horseradish peroxidase, and infrared peroxidase substrate stock were prepared and kept in a dark and cold (0 °C) environment. Second, 0 to 100 μM hydrogen peroxide solutions were made by diluting the 30% solution from Sigma (95321, Sigma-Aldrich). Third, 50 μL H_2O_2 standards and 50 μL detection reagent were mixed and transferred to a 96 well black wall plate (655090, Greiner Bio-One International GmbH). Afterward, the samples were incubated for 15−30 min, and the fluorescence was measured with the microplate reader (same as before, excitation: 540 nm; emission: 590 nm). Calibration curves for H_2O_2 in liquid water and SLF were obtained and shown in Figure S6. The concentration of SOA used for the H_2O_2 yield test was 100 μM for all the samples. We also measured 0.5−22 μM cumene hydroperoxides and *tert*-butyl hydroperoxide with the H_2O_2 assay kit, which generated no fluorescence, confirming the high selectivity of the assay toward H_2O_2 rather than organic hydroperoxides.

Kinetic Modeling. The production rates of radicals shown in Figure 6 (panels a and b) were modeled using the mechanism and reactions shown in Table S2. The reactions in the model included the decomposition of ROOH, the reaction of semiquinones with oxygen, HO_x chemistry, reactions of antioxidants with reactive oxygen species, reactions of TEMPONE-H with reactive oxygen species, and the self-reaction of the TEMPONE radical. Literature rate constants were used for the majority of these reactions, but when they were unknown or

DOI: 10.1021/acs.est.8b03695
Environ. Sci. Technol. 2018, 52, 11642−11651

Table 1. H_2O_2 Yields by Ambient Particles and Laboratory Generated SOA

type of samples	H_2O_2 yield in H_2O		H_2O_2 yield in SLF		ref
	molar yield (%)	per mass (ng/μg)	molar yield (%)	per mass (ng/μg)	
Ambient Fine, UCLA, 2005−2006	0.25 ± 0.18	0.42 ± 0.30			60
Ambient Fine, Downtown LA, 2005−2006	0.34 ± 0.18	0.58 ± 0.31			60
Ambient Fine, Riverside, UCR	0.56 ± 0.41	0.95 ± 0.69			59
Ambient Fine, Riverside, CRCAES	0.29 ± 0.32	0.49 ± 0.55			59
Ambient Fine, UCLA, 2009−2010	0.06 ± 0.04	0.11 ± 0.07			59
Diesel Idle	0.11 ± 0.15	0.19 ± 0.26			59
Diesel Load	0.035 ± 0.05	0.06 ± 0.08			59
Biodiesel Idle	0.28 ± 0.1	0.48 ± 0.17			59
Biodiesel Load	0.19 ± 0.09	0.33 ± 0.16			59
α-pinene SOA	0.55 ± 0.21	0.93 ± 0.36			59
β-pinene SOA	1.25 ± 0.87	2.12 ± 1.48			59
Isoprene SOA	7.98 ± 0.75	13.56 ± 1.27	2.66 ± 0.05	4.52 ± 0.08	this study
β-pinene SOA	3.22 ± 0.73	5.47 ± 1.24	1.21 ± 0.05	2.05 ± 0.09	this study
Naphthalene SOA	0.67 ± 0.66	1.91 ± 0.33	9.58 ± 2.61	16.3 ± 4.4	this study

uncertain, the rate constants were determined using the Monte Carlo genetic algorithm[51] and sensitivity tests. In addition to the chemistry shown in Table S2, a H_2O_2 production rate was included in the model. These production rates were based upon the molar H_2O_2 yields that had been measured of 2.66%, 1.21%, and 9.58% for isoprene, β-pinene, and naphthalene SOA in SLF, respectively, and 7.98%, 3.22%, and 0.67% for isoprene, β-pinene, and naphthalene SOA in water as shown in Table 1.

RESULTS AND DISCUSSION

EPFR and ROS Formation in Water. Direct EPR measurements of SOA particles collected on Teflon filters (without extraction) are shown with green lines in Figure 2. They indicate that isoprene (spectrum A) and β-pinene (spectrum D) SOA do not contain any stable radicals. Naphthalene SOA (spectrum G) contain stable radicals with a g-factor of 2.0045, which is consistent with EPFR with a chemical identity of semiquinone radicals.[52,53] The total number of spins in naphthalene SOA that was collected at 30% RH (N_{-S}) was quantified as a function of naphthalene SOA mass as shown in Figure 3a. The N_{-S} increases linearly at higher naphthalene SOA mass, and the average EPFR concentration is 1.36 (±0.18) × 10^{11} spins μg^{-1}, which is the same order of magnitude as the EPFR in field particles.[11] This indicates that oxidation of PAH with OH may be one of the efficient pathways of producing EPFR. Previous studies have shown that heterogeneous ozonolysis of polycyclic aromatic hydrocarbons can lead to the formation of long-lived reactive oxygen intermediates or EPFR.[34,35]

Decay of EPFR was measured at two different temperatures of 295 and 241 K. The chemical half-life of semiquinone radicals in naphthalene SOA was found to be 2 h at both 295 (30% RH) and 241 K (52% RH) (Figure 3b). This lifetime is on the same order of time scale as the phenoxy- and semiquinone-type radicals formed on metal oxide surfaces[54] but is shorter than ambient particles, which have a longer lifetime of 1 day to weeks.[32,33] Furthermore, the peak area and intensity of the EPR spectra associated with these EPFR decreased rapidly over 5 min upon exposure to a humidified nitrogen flow at a RH 52% as shown in Figure 3c. This indicates that EPFR have a longer lifetime under dry conditions, and they may decompose upon interaction with water. This result is consistent with the study by Jia et al.,[33] which showed a fast decay of anthracene source EPFR even under 8% RH.

Figure 2 also includes EPR measurements with a spin-trapping technique for SOA water extracts mixed with BMPO (pink lines). For better evaluation of different types of radicals and radical adducts, we used the spin fitting module in Xenon software to obtain the deconvolution of EPR spectra and showed the simulated spectra for ascorbate radicals, BMPO-OH, BMPO-OOH, BMPO-OR, and BMPO-R in Figure 2d. On the basis of these simulated spectra, we assigned the spectra peaks in panels a to c to different types of radical or radical adduct species, which were labeled with dashed lines. Figure 2 (panels a and b) shows that isoprene (spectrum B) and β-pinene SOA (spectrum E) generated OH, $O_2^{\bullet-}$, and organic radicals, whereas naphthalene SOA (spectrum H) yielded $O_2^{\bullet-}$ and organic radicals but not OH radicals. The presence of these radicals was also confirmed by LC−MS/MS analysis (see Table S1 and Figure S1).

To explore the correlation of peroxide contents with ROS formation, the total peroxides in SOA were determined by a iodometric-spectrophotometric method.[50] It was found that organic peroxides in isoprene, β-pinene, and naphthalene SOA accounted for approximately 95(±28)%, 42(±24)%, and 19(±7)% of the total mass of the SOA, respectively (Figure 4a), which are on the same order with previous studies,[50,55,56] even though the measured abundance of total peroxides in SOA by different studies varies due to different formation conditions and also different freshness of collected particles.

The molar yields of total radicals (OH, $O_2^{\bullet-}$, organic radicals) and relative yield of each adduct are shown in Figure 4b and Figure 5, respectively. Figure 4b shows that the total radical yields by isoprene, β-pinene, and naphthalene SOA were around 3.8%, 5.2%, and 1.1%, respectively. It also indicates that the radical production rates of SOA in water appears to be related with the abundance of total peroxides in SOA (Figure 4a), implying that the generation of OH and organic radicals by isoprene, β-pinene, and naphthalene SOA may be induced by the decomposition of organic hydroperoxides. Figure 5 indicates that OH accounts for 70% and 66% of generated radicals for isoprene and β-pinene SOA, respectively. $O_2^{\bullet-}$ is the dominant product with yields of 83% for naphthalene SOA. $O_2^{\bullet-}$ is most likely generated by redox reactions of semiquinones contained in naphthalene SOA ($SQ^{\bullet} + O_2 \leftrightharpoons Q + O_2^{\bullet-}$).[57]

DOI: 10.1021/acs.est.8b03695
Environ. Sci. Technol. 2018, 52, 11642−11651

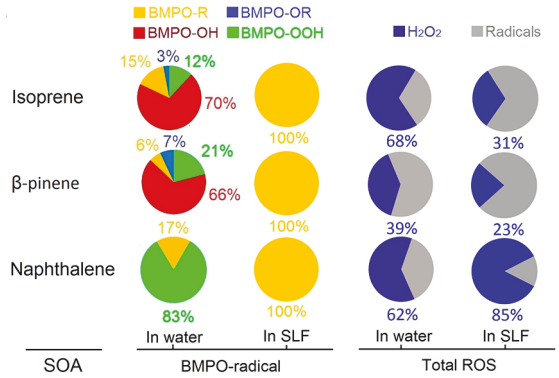

Figure 5. Relative yields of BMPO-radical adducts and total ROS (sum of H_2O_2 and total radicals) in water and SLF by isoprene, β-pinene, and naphthalene SOA. Different colors were used to indicate different types of radical species. Gray part of the pie chart for yields of total radicals are based on TEMPONE radical yields with TEMPONE-H as the spin trap. The initial concentration of SOA in water and SLF extract is 1 mM. More details about the composition of SLF and extraction methods were given in the Experimental Section and Supporting Information.

Naphthalene SOA generated very little OH radicals, which is consistent with low concentrations of organic peroxides.

Furthermore, we also found that isoprene, β-pinene, and naphthalene SOA generated substantial amounts of H_2O_2 upon interaction with water. Combining the measurements using EPR for radicals with a fluorimetric assay for H_2O_2, Figure 4c shows molar yields of total ROS by SOA in liquid water after approximately 10 min. Isoprene SOA showed the highest molar yield of around 12%, followed by β-pinene SOA of 8%, and naphthalene SOA of 2%. The total ROS yield of β-pinene SOA is about two times higher compared to the ROS yield of α-pinene SOA by Chen et al. using a fluorogenic probe composed of dichlorofluorescin (DCFH) and horseradish peroxidase.[58]

Figure 5 shows that H_2O_2 is the most abundant ROS species formed by isoprene and naphthalene SOA, which contributes approximately 68% and 62% toward the total ROS yield in pure water. In contrast, H_2O_2 contributes 39% of totally formed ROS by β-pinene SOA, and radicals are dominant. The order of the total ROS yield of SOA (isoprene > β-pinene > naphthalene, Figure 4c) matches with the total peroxide abundance of SOA and molar yield of total radicals as shown in Figure 4 (panels a and b), indicating the plausible role of organic hydroperoxides as the precursor of aqueous ROS generated by isoprene, β-pinene, and naphthalene SOA.[10] This finding is also in agreement with the recent study by Kramer et al. in 2016 showing that isoprene epoxydiols (IEPOX) and isoprene derived hydroxyhydroperoxide have a high ROS generation potential.[47]

The H_2O_2 yield of SOA in liquid water has been compared with that of SOA and ambient particles from previous studies as shown in Table 1. For the production of H_2O_2 by β-pinene SOA, a molar yield of 3.2% was observed in this study, which is around 1.6 times higher than the result from Wang et al.,[59] who generated SOA with lower oxidant concentrations. This study provides first measurements of H_2O_2 molar yields of isoprene and naphthalene SOA as 8.0% and 0.67%, respectively. Molar H_2O_2 yields from SOA are much higher than those by diesel and ambient fine particles with the H_2O_2 yield ranging 0.035−0.56% (Table 1),[59,60] indicating that SOA may play a significant role in the formation of H_2O_2 in ambient particles or cloud droplets.

ROS Formation by SOA in Surrogate Lung Fluid (SLF). To evaluate potential adverse health effects of SOA upon respiratory deposition, we quantified ROS formation by isoprene, β-pinene, and naphthalene SOA in SLF[61] using EPR combined with spin trapping and probing techniques. SLF contains ascorbate, uric acid, and glutathione, which are lung antioxidants, as well as citric acid in phosphate-buffered saline with a pH of 7.4 (for more details see Experimental Section). The EPR spectra of such measurements are shown in Figure 2 (panels a to c) with black lines. Upon interaction with SLF, isoprene and β-pinene SOA mainly released organic radicals (marked with brown dashed lines), while OH radicals that were prominently observed in liquid water were all scavenged by antioxidants, as evident from the formation of ascorbate radicals (as indicated by the black dashed lines). Organic radicals that are not scavenged by antioxidants might be harmful in the lung as they can cause peroxidation[62] of lipids including the pulmonary lipids.[63] Naphthalene SOA did not form substantial amounts of radicals, which may be due to the lower abundance of organic hydroperoxides and depletion of radicals (which may be formed via redox reactions of semiquinones) by antioxidants or secondary chemistry of radical adducts that may lead to decomposition of radical adducts.[42]

The radical and H_2O_2 yields of SOA in SLF are shown in Figure 4 (panels b and c) and 5. The total radical yields of isoprene, β-pinene, and naphthalene SOA when using TEMPONE-H as the spin probing agent are around 5.8%, 4.0%, and 1.7%, respectively (Figure 4b). Furthermore, we also found that SOA generated substantial amounts of H_2O_2 upon interaction with SLF. The total ROS generation yields of isoprene (8.5%) and β-pinene (5.2%) SOA in SLF (Figure 4c) are slightly lower than those in liquid water (11.8% and 8.2%, Figure 4b) due to scavenging of ROS (mainly radicals) by antioxidants. Isoprene and β-pinene SOA contain substantial amount of organic hydroperoxides that can decompose in aqueous solutions and form H_2O_2.[64] On the basis of different cleavage pathways for organic hydroperoxide decomposition and further reactions of organic radicals, OH and superoxide radicals may be generated.[65,66] Then H_2O_2 can be formed by recombination of OH radicals ($OH + OH \rightarrow H_2O_2$, R5) or protonation of superoxide radicals ($HO_2 + HO_2 \rightarrow H_2O_2 + O_2$, R7). The strong ability of antioxidants to scavenge OH and superoxide radicals (Figure 2) and the decreased radical and H_2O_2 yields of isoprene SOA and β-pinene in SLF (Table 1, Figure 4 (panels b and c), and Figure 5) are consistent with this hypothesis. Interestingly, naphthalene SOA generated more H_2O_2 in SLF (9.6%) than that in liquid water (0.7%, Figure 4c). This may be explained by the relatively high concentration of redox-active quinones[67] and the formation of H_2O_2 from their interaction with antioxidants.[61] The low BMPO-OOH but high molar H_2O_2 yield of naphthalene SOA in SLF (Figure 5) may be related to the increased stabilization of semiquinones induced by a prohibited protonation and reduction at pH = 7.4,[68] which may lead to higher concentrations of semiquinones and thus higher yields of H_2O_2. On the other hand, the increased radical concentrations may cause BMPO-$O_2^{\bullet-}$ adducts to decay by radical reactions,[42] decreasing the detectability of BMPO-OOH.[69]

ROS Yield versus Oxidative Potential of SOA. We measured the DTT consumption rates by isoprene, β-pinene, and naphthalene SOA (Table S3), which are

DOI: 10.1021/acs.est.8b03695
Environ. Sci. Technol. 2018, 52, 11642−11651

considered as a proxy for redox activity and oxidative potential. Naphthalene SOA showed the highest DTT decay rates of 104.4(±7.6) pmol min^{-1} μg^{-1}, which are very similar to previously reported values.[20,25,69] In contrast, isoprene and β-pinene SOA showed lower DTT consumption rate with values of 48.3(±7.9) and 36.4(±3.1) pmol min^{-1} μg^{-1}, respectively, which is similar to values for ambient organic particles.[70] The DTT consumption rate by isoprene SOA formed in the PAM chamber in this study was measured to be higher than isoprene SOA formed in a smog chamber (Tuet et al., 2017) and ambient isoprene-derived OA (8.8(±21) pmol min^{-1} μg^{-1})[70] as estimated by a positive matrix factorization analysis. This difference may be due to difference in reaction conditions such as different UV light sources, oxidant, and relative humidity, and oxidant and precursor concentrations in our study are much higher than chamber or ambient conditions.

The order of DTT decay rates of naphthalene > isoprene > β-pinene does not match the order of ROS yield in water but matches with H_2O_2 and total ROS yield in SLF (Figure S7). This indicates that H_2O_2 yield is closely related with the redox activity of SOA, which is in agreement with previous studies.[71,72] The high oxidative potential of naphthalene SOA indicate that EPFR and quinones may play a role in generating superoxide and carbon-cantered radicals in water. In this study, we did not observe clear relations of DTT decay rates with the yields of radical adducts including OH, superoxide, and organic radicals. Interactions and coupling of redox-active compounds, ROS, and antixodants/DTT are complex and further experiments are warranted in future studies.

ROS Generation Rates by SOA and Kinetic Modeling. Figure 6 (panels a and b) shows the ROS production rates as a function of SOA concentration in water. Isoprene SOA shows the largest ROS production rate (~179 nM s^{-1} mM^{-1} SOA), followed by β-pinene (~102 nM s^{-1} mM^{-1} SOA) and naphthalene (~38 nM s^{-1} mM^{-1} SOA) in water. In order to obtain a better understanding of the mechanism of ROS formation by SOA upon reactions in liquid water, we developed a kinetic box model to simulate reactions, including the decomposition of ROOH (ROOH → $RO^{\bullet}$ + $^{\bullet}OH$), redox-cycling between quinones and semiquinones (e.g., $AscH^-$ + Q → $SQ^{\bullet}$ + Asc^- and $SQ^{\bullet}$ + O_2 → Q + $O_2^{\bullet-}$), and HO_x chemistry (Table S2 and Supporting Information). Within the model we assumed that 15% of the total isoprene and β-pinene SOA consisted of ROOH that would decompose to form radicals, while we assumed that 10% of the naphthalene SOA consisted of semiquinones that would produce ROS. The experimental results were modeled as shown by the lines that fit the experimental data very well. Model simulations confirm that the dominant radical formation process should be ROOH decomposition for isoprene and β-pinene SOA, while semiquinone reactions with oxygen (see Table S2 or the Experimental Section for the detailed mechanism) are the main source of radicals for naphthalene SOA.

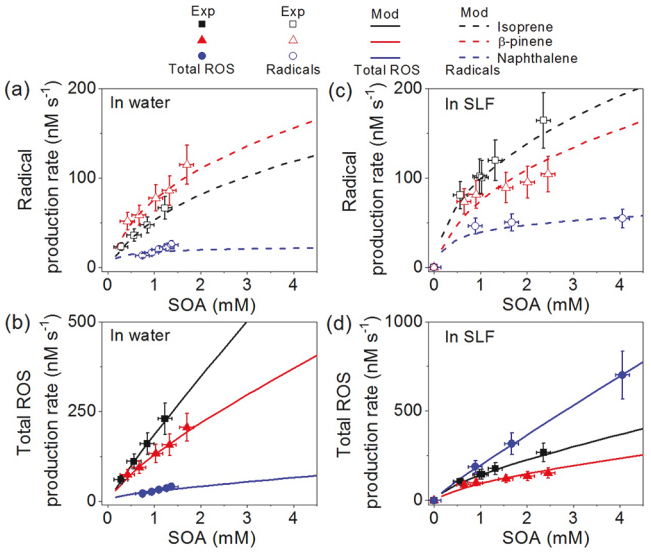

Figure 6. (a and c) Average radical and (b and d) total ROS production rates by SOA in (a and b) water and (c and d) SLF in initial 10 min of reactions. The filled points are the measured total ROS production rates, and the hollow points are the measured production rates of radicals by isoprene (black), β-pinene (red), and naphthalene (blue) SOA. The solid and dashed lines represent the modeled total ROS and radical production rates, respectively.

The experimental and modeled ROS production rates of isoprene, β-pinene, and naphthalene SOA in SLF are shown in Figure 6 (panels c and d). Figure 6c indicates that isoprene SOA shows the largest radical production rate (~65 nM s^{-1} mM^{-1} SOA), followed by β-pinene (~35 nM s^{-1} mM^{-1} SOA) and naphthalene (~11 nM s^{-1} mM^{-1} SOA). Figure 6d shows the production rates of total ROS by SOA in SLF, which are also in agreement with the modeled data, showing a positive relationship of total ROS production rates with SOA concentrations. Overall Figure 6 indicates that ROS production by SOA in water and SLF are quite different, and modeled results are in agreement with the experimental observations for the production of trapped radicals with TEMPONE-H as the spin trap. In liquid water, the aqueous phase chemistry of isoprene and β-pinene SOA is dominated by the decomposition of ROOH (R1) and the decomposition of other species which form H_2O_2 (see the Supporting Information), leading to the formation of substantial amounts of H_2O_2, OH, and organic radicals. Whereas naphthalene SOA contains less organic peroxides but relatively high concentrations of quinone and semiquinone compounds, which may react with dissolved O_2 to form $O_2^{\bullet-}$ and H_2O_2. Note that these fractions of ROOH and semiquinones within the SOA were codependent with the rate coefficients of reactions R1 (ROOH → $RO^{\bullet}$ + $^{\bullet}OH$) and R30 ($SQ^{\bullet}$ + O_2 → Q + $O_2^{\bullet-}$, e.g., the measurements could still be reproduced if the fraction of ROOH within the SOA was increased if the rate constant k_1 was decreased). In SLF, antioxidants scavenge OH, $O_2^{\bullet-}$, and organic radicals. However, naphthalene SOA shows a substantial increase in ROS production, especially the H_2O_2 production rate, due to sustained redox reactions between semiquinones and antioxidants (R30). Interestingly, the production rates of radicals by SOA within the SLF were generally higher than that in water, suggesting that the decomposition of ROOH was pH-dependent and that TEMPONE-H trapped radicals efficiently before radicals were reacted away by antioxidants.

These results indicate that SOA derived from both biogenic and anthropologic volatile compounds can form substantial amounts of radicals and H_2O_2 in lung lining fluid, especially naphthalene SOA can release substantial amounts of $O_2^{\bullet-}$ and H_2O_2. It is known that excess amounts of ROS can cause oxidative stress to the human lung and induce a broad range of toxicological effects.[4,73,74] Previous studies have indicated that typical H_2O_2 concentrations of exhaled breath condensate from patients with different respiratory tract diseases are in the

DOI: 10.1021/acs.est.8b03695
Environ. Sci. Technol. 2018, 52, 11642−11651

range of 100−200 nM.[75−82] Therefore, an increase in the molar H_2O_2 and ROS yield from increased SOA concentrations has the potential to increase ROS concentrations in the SLF to harmful levels in many of the more polluted cities. Thus, inhalation of fresh SOA particles, which have the potential to release high levels of H_2O_2 and ROS, may have significant adverse health effects, especially in polluted indoor air or urban megacities with high SOA concentrations. A very recent study has shown that aged SOA may have higher toxicological effects than fresh SOA,[73] which may warrant further studies on ROS formation by aged SOA particles.

■ ASSOCIATED CONTENT

Supporting Information

The Supporting Information is available free of charge on the ACS Publications website at DOI: 10.1021/acs.est.8b03695.

Radicals identified with LC−MS/MS; equations and parameters used in the kinetic model for ROS generation; compiled oxidative potentials of different types of SOA from the current study and literature; identification by LC−MS/MS, MS^2 spectra, and proposed fragmentation pathways; calibration curve and oxidation potentials of SOA characterized with DTT; EPR spectra; pH values of SOA with different concentrations; calibration curve for total peroxides of SOA measurement; calibration curve used to quantify the H_2O_2 yield of SOA; and H_2O_2 yield in SLF vs the DTT consumption rate of SOA (PDF)

■ AUTHOR INFORMATION

Corresponding Authors

*email: h.tong@mpic.de.
*email: m.shiraiwa@uci.edu.

ORCID

Haijie Tong: 0000-0001-9887-7836
Manabu Shiraiwa: 0000-0003-2532-5373

Notes

The authors declare no competing financial interest.

■ ACKNOWLEDGMENTS

This work was funded by the Max Planck Society. M.S. acknowledges funding from the National Science Foundation (CHE-1808125).

■ REFERENCES

(1) Hallquist, M.; Wenger, J. C.; Baltensperger, U.; Rudich, Y.; Simpson, D.; Claeys, M.; Dommen, J.; Donahue, N. M.; George, C.; Goldstein, A. H.; Hamilton, J. F.; Herrmann, H.; Hoffmann, T.; Iinuma, Y.; Jang, M.; Jenkin, M. E.; Jimenez, J. L.; Kiendler-Scharr, A.; Maenhaut, W.; McFiggans, G.; Mentel, T. F.; Monod, A.; Prévôt, A. S. H.; Seinfeld, J. H.; Surratt, J. D.; Szmigielski, R.; Wildt, J. The formation, properties and impact of secondary organic aerosol: current and emerging issues. *Atmos. Chem. Phys.* **2009**, *9* (14), 5155−5236.

(2) Ziemann, P. J.; Atkinson, R. Kinetics, products, and mechanisms of secondary organic aerosol formation. *Chem. Soc. Rev.* **2012**, *41* (19), 6582−6605.

(3) Nozière, B.; Kalberer, M.; Claeys, M.; Allan, J.; D'Anna, B.; Decesari, S.; Finessi, E.; Glasius, M.; Grgić, I.; Hamilton, J. F.; Hoffmann, T.; Iinuma, Y.; Jaoui, M.; Kahnt, A.; Kampf, C. J.; Kourtchev, I.; Maenhaut, W.; Marsden, N.; Saarikoski, S.; Schnelle-Kreis, J.; Surratt, J. D.; Szidat, S.; Szmigielski, R.; Wisthaler, A. The Molecular Identification of Organic Compounds in the Atmosphere: State of the Art and Challenges. *Chem. Rev.* **2015**, *115* (10), 3919−3983.

(4) Pöschl, U.; Shiraiwa, M. Multiphase chemistry at the atmosphere-biosphere interface influencing climate and public health in the anthropocene. *Chem. Rev.* **2015**, *115* (10), 4440−4475.

(5) Winterbourn, C. C. Reconciling the chemistry and biology of reactive oxygen species. *Nat. Chem. Biol.* **2008**, *4* (5), 278−286.

(6) Lakey, P. S. J.; Berkemeier, T.; Tong, H.; Arangio, A. M.; Lucas, K.; Pöschl, U.; Shiraiwa, M. Chemical exposure-response relationship between air pollutants and reactive oxygen species in the human respiratory tract. *Sci. Rep.* **2016**, *6*, 32916.

(7) Charrier, J. G.; Anastasio, C. Rates of Hydroxyl Radical Production from Transition Metals and Quinones in a Surrogate Lung Fluid. *Environ. Sci. Technol.* **2015**, *49* (15), 9317−9325.

(8) Dou, J.; Lin, P.; Kuang, B.-Y.; Yu, J. Z. Reactive Oxygen Species Production Mediated by Humic-like Substances in Atmospheric Aerosols: Enhancement Effects by Pyridine, Imidazole, and Their Derivatives. *Environ. Sci. Technol.* **2015**, *49* (11), 6457−6465.

(9) Gonzalez, D. H.; Cala, C. K.; Peng, Q.; Paulson, S. E. HULIS Enhancement of Hydroxyl Radical Formation from Fe(II): Kinetics of Fulvic Acid−Fe(II) Complexes in the Presence of Lung Antioxidants. *Environ. Sci. Technol.* **2017**, *51* (13), 7676−7685.

(10) Tong, H.; Arangio, A.; Lakey, P.; Berkemeier, T.; Liu, F.; Kampf, C.; Brune, W. H.; Pöschl, U.; Shiraiwa, M. Hydroxyl radicals from secondary organic aerosol decomposition in water. *Atmos. Chem. Phys.* **2016**, *16*, 1761−1771.

(11) Arangio, A. M.; Tong, H.; Socorro, J.; Pöschl, U.; Shiraiwa, M. Quantification of environmentally persistent free radicals and reactive oxygen species in atmospheric aerosol particles. *Atmos. Chem. Phys.* **2016**, *16* (20), 13105−13119.

(12) Gehling, W.; Khachatryan, L.; Dellinger, B. Hydroxyl radical generation from environmentally persistent free radicals (EPFRs) in PM2. 5. *Environ. Sci. Technol.* **2014**, *48* (8), 4266−4272.

(13) Fuller, S. J.; Wragg, F. P. H.; Nutter, J.; Kalberer, M. Comparison of on-line and off-line methods to quantify reactive oxygen species (ROS) in atmospheric aerosols. *Atmos. Environ.* **2014**, *92*, 97−103.

(14) Charrier, J. G.; Anastasio, C. On dithiothreitol (DTT) as a measure of oxidative potential for ambient particles: evidence for the importance of soluble transition metals. *Atmos. Chem. Phys.* **2012**, *12* (19), 9321−9333.

(15) Landreman, A. P.; Shafer, M. M.; Hemming, J. C.; Hannigan, M. P.; Schauer, J. J. A macrophage-based method for the assessment of the reactive oxygen species (ROS) activity of atmospheric particulate matter (PM) and application to routine (daily-24 h) aerosol monitoring studies. *Aerosol Sci. Technol.* **2008**, *42* (11), 946−957.

(16) Fang, T.; Verma, V.; Bates, J. T.; Abrams, J.; Klein, M.; Strickland, M. J.; Sarnat, S. E.; Chang, H. H.; Mulholland, J. A.; Tolbert, P. E.; Russell, A. G.; Weber, R. J. Oxidative potential of ambient water-soluble PM 2.5 measured by Dithiothreitol (DTT) and Ascorbic Acid (AA) assays in the southeastern United States: contrasts in sources and health associations. *Atmos. Chem. Phys.* **2016**, *16* (6), 3865−3879.

(17) Sameenoi, Y.; Koehler, K.; Shapiro, J.; Boonsong, K.; Sun, Y.; Collett, J., Jr; Volckens, J.; Henry, C. S. Microfluidic electrochemical sensor for on-line monitoring of aerosol oxidative activity. *J. Am. Chem. Soc.* **2012**, *134* (25), 10562−10568.

(18) McWhinney, R. D.; Badali, K.; Liggio, J.; Li, S.-M.; Abbatt, J. P. D. Filterable redox cycling activity: a comparison between diesel exhaust particles and secondary organic aerosol constituents. *Environ. Sci. Technol.* **2013**, *47* (7), 3362−3369.

(19) Lin, Y.-H.; Arashiro, M.; Martin, E.; Chen, Y.; Zhang, Z.; Sexton, K. G.; Gold, A.; Jaspers, I.; Fry, R. C.; Surratt, J. D. Isoprene-Derived Secondary Organic Aerosol Induces the Expression of Oxidative Stress Response Genes in Human Lung Cells. *Environ. Sci. Technol. Lett.* **2016**, *3*, 250−254.

(20) Tuet, W. Y.; Chen, Y.; Xu, L.; Fok, S.; Gao, D.; Weber, R. J.; Ng, N. L. Chemical oxidative potential of secondary organic aerosol

DOI: 10.1021/acs.est.8b03695
Environ. Sci. Technol. 2018, 52, 11642−11651

(SOA) generated from the photooxidation of biogenic and anthropogenic volatile organic compounds. *Atmos. Chem. Phys.* **2017**, *17* (2), 839−853.
(21) Li, N.; Sioutas, C.; Cho, A.; Schmitz, D.; Misra, C.; Sempf, J.; Wang, M.; Oberley, T.; Froines, J.; Nel, A. Ultrafine particulate pollutants induce oxidative stress and mitochondrial damage. *Environ. Health Perspect.* **2002**, *111* (4), 455−460.
(22) Velali, E.; Papachristou, E.; Pantazaki, A.; Choli-Papadopoulou, T.; Planou, S.; Kouras, A.; Manoli, E.; Besis, A.; Voutsa, D.; Samara, C. Redox activity and in vitro bioactivity of the water-soluble fraction of urban particulate matter in relation to particle size and chemical composition. *Environ. Pollut.* **2016**, *208*, 774−786.
(23) Liu, Q.; Baumgartner, J.; Zhang, Y.; Liu, Y.; Sun, Y.; Zhang, M. Oxidative potential and inflammatory impacts of source apportioned ambient air pollution in Beijing. *Environ. Sci. Technol.* **2014**, *48* (21), 12920−12929.
(24) Li, Q.; Wyatt, A.; Kamens, R. M. Oxidant generation and toxicity enhancement of aged-diesel exhaust. *Atmos. Environ.* **2009**, *43* (5), 1037−1042.
(25) Wang, S.; Ye, J.; Soong, R.; Wu, B.; Yu, L.; Simpson, A. J.; Chan, A. W. Relationship between chemical composition and oxidative potential of secondary organic aerosol from polycyclic aromatic hydrocarbons. *Atmos. Chem. Phys.* **2018**, *18* (6), 3987−4003.
(26) Delfino, R. J.; Staimer, N.; Tjoa, T.; Gillen, D. L.; Schauer, J. J.; Shafer, M. M. Airway inflammation and oxidative potential of air pollutant particles in a pediatric asthma panel. *J. Exposure Sci. Environ. Epidemiol.* **2013**, *23* (5), 466−473.
(27) Yang, A.; Janssen, N. A.; Brunekreef, B.; Cassee, F. R.; Hoek, G.; Gehring, U. Children's respiratory health and oxidative potential of PM2. 5: the PIAMA birth cohort study. *Occup. Environ. Med.* **2016**, *73* (3), 154−160, DOI: 10.1136/oemed-2015-103175.
(28) Shiraiwa, M.; Ueda, K.; Pozzer, A.; Lammel, G.; Kampf, C. J.; Fushimi, A.; Enami, S.; Arangio, A. M.; Fröhlich-Nowoisky, J.; Fujitani, Y.; Furuyama, A.; Lakey, P. S. J.; Lelieveld, J.; Lucas, K.; Morino, Y.; Pöschl, U.; Takahama, S.; Takami, A.; Tong, H.; Weber, B.; Yoshino, A.; Sato, K. Aerosol health effects from molecular to global scales. *Environ. Sci. Technol.* **2017**, *51* (23), 13545−13567.
(29) Tong, H.; Lakey, P.; Arangio, A.; Socorro, J.; Kampf, C. J.; Berkemeier, T.; Brune, W. H.; Pöschl, U.; Shiraiwa, M. Reactive oxygen species formed in aqueous mixtures of secondary organic aerosols and mineral dust influencing cloud chemistry and public health in the Anthropocene. *Faraday Discuss.* **2017**, *200*, 251−270.
(30) Badali, K.; Zhou, S.; Aljawhary, D.; Antiñolo, M.; Chen, W.; Lok, A.; Mungall, E.; Wong, J.; Zhao, R.; Abbatt, J. Formation of hydroxyl radicals from photolysis of secondary organic aerosol material. *Atmos. Chem. Phys.* **2015**, *15* (4), 7831−7840.
(31) Dellinger, B.; Lomnicki, S.; Khachatryan, L.; Maskos, Z.; Hall, R. W.; Adounkpe, J.; McFerrin, C.; Truong, H. Formation and stabilization of persistent free radicals. *Proc. Combust. Inst.* **2007**, *31* (1), 521−528.
(32) Gehling, W.; Dellinger, B. Environmentally persistent free radicals and their lifetimes in $PM_{2.5}$. *Environ. Sci. Technol.* **2013**, *47* (15), 8172−8178.
(33) Jia, H.; Nulaji, G.; Gao, H.; Wang, F.; Zhu, Y.; Wang, C. Formation and stabilization of environmentally persistent free radicals induced by the interaction of anthracene with Fe (III)-modified clays. *Environ. Sci. Technol.* **2016**, *50* (12), 6310−6319.
(34) Shiraiwa, M.; Sosedova, Y.; Rouvière, A.; Yang, H.; Zhang, Y.; Abbatt, J. P. D.; Ammann, M.; Pöschl, U. The role of long-lived reactive oxygen intermediates in the reaction of ozone with aerosol particles. *Nat. Chem.* **2011**, *3* (4), 291−295.
(35) Borrowman, C. K.; Zhou, S.; Burrow, T. E.; Abbatt, J. P. D. Formation of environmentally persistent free radicals from the heterogeneous reaction of ozone and polycyclic aromatic compounds. *Phys. Chem. Chem. Phys.* **2016**, *18* (1), 205−212.
(36) Balakrishna, S.; Lomnicki, S. M.; McAvey, K. M.; Cole, R. B.; Dellinger, B.; Cormier, S. A. Environmentally persistent free radicals amplify ultrafine particle mediated cellular oxidative stress and cytotoxicity. *Part. Fibre Toxicol.* **2009**, *6* (1), 11.
(37) Kang, E.; Root, M.; Toohey, D.; Brune, W. Introducing the concept of potential aerosol mass (PAM). *Atmos. Chem. Phys.* **2007**, *7* (22), 5727−5744.
(38) Peng, Z.; Day, D. A.; Ortega, A. M.; Palm, B. B.; Hu, W.; Stark, H.; Li, R.; Tsigaridis, K.; Brune, W. H.; Jimenez, J. L. Non-OH chemistry in oxidation flow reactors for the study of atmospheric chemistry systematically examined by modeling. *Atmos. Chem. Phys.* **2016**, *16* (7), 4283−4305.
(39) Lambe, A. T.; Chhabra, P. S.; Onasch, T. B.; Brune, W. H.; Hunter, J. F.; Kroll, J. H.; Cummings, M. J.; Brogan, J. F.; Parmar, Y.; Worsnop, D. R.; Kolb, C. E.; Davidovits, P. Effect of oxidant concentration, exposure time, and seed particles on secondary organic aerosol chemical composition and yield. *Atmos. Chem. Phys.* **2015**, *15* (6), 3063−3075.
(40) Bruns, E. A.; El Haddad, I.; Keller, A.; Klein, F.; Kumar, N. K.; Pieber, S. M.; Corbin, J. C.; Slowik, J. G.; Brune, W. H.; Baltensperger, U.; Prévôt, A. S. H. Inter-comparison of laboratory smog chamber and flow reactor systems on organic aerosol yield and composition. *Atmos. Meas. Tech.* **2015**, *8* (6), 2315−2332.
(41) Stoll, S.; Schweiger, A. EasySpin, a comprehensive software package for spectral simulation and analysis in EPR. *J. Magn. Reson.* **2006**, *178* (1), 42−55.
(42) Zhao, H.; Joseph, J.; Zhang, H.; Karoui, H.; Kalyanaraman, B. Synthesis and biochemical applications of a solid cyclic nitrone spin trap: a relatively superior trap for detecting superoxide anions and glutathiyl radicals. *Free Radical Biol. Med.* **2001**, *31* (5), 599−606.
(43) Dikalov, S.; Skatchkov, M.; Bassenge, E. Quantification of peroxynitrite, superoxide, and peroxyl radicals by a new spin trap hydroxylamine 1-hydroxy-2, 2, 6, 6-tetramethyl-4-oxo-piperidine. *Biochem. Biophys. Res. Commun.* **1997**, *230* (1), 54−57.
(44) Rosen, G. M.; Tsai, P.; Weaver, J.; Porasuphatana, S.; Roman, L. J.; Starkov, A. A.; Fiskum, G.; Pou, S. The role of tetrahydrobiopterin in the regulation of neuronal nitric-oxide synthase-generated superoxide. *J. Biol. Chem.* **2002**, *277* (43), 40275−40280.
(45) Weber, R. T. *Xenon Data Processing Reference*; Bruker Instruments: Billerica, MA, 2012.
(46) Eaton, G. R.; Eaton, S. S.; Barr, D. P.; Weber, R. T. *Quantitative EPR*; Springer Science & Business Media, 2010.
(47) Kramer, A. J.; Rattanavaraha, W.; Zhang, Z.; Gold, A.; Surratt, J. D.; Lin, Y.-H. Assessing the oxidative potential of isoprene-derived epoxides and secondary organic aerosol. *Atmos. Environ.* **2016**, *130*, 211−218.
(48) Fang, T.; Verma, V.; Guo, H.; King, L. E.; Edgerton, E. S.; Weber, R. J. A semi-automated system for quantifying the oxidative potential of ambient particles in aqueous extracts using the dithiothreitol (DTT) assay: results from the Southeastern Center for Air Pollution and Epidemiology (SCAPE). *Atmos. Meas. Tech.* **2015**, *8* (1), 471−482.
(49) Jiang, H.; Jang, M.; Sabo-Attwood, T.; Robinson, S. E. Oxidative Potential of Secondary Organic Aerosols Produced from Photooxidation of Different Hydrocarbons Using Outdoor Chamber under Ambient Sunlight. *Atmos. Environ.* **2016**, *131*, 382−389.
(50) Docherty, K. S.; Wu, W.; Lim, Y. B.; Ziemann, P. J. Contributions of organic peroxides to secondary aerosol formed from reactions of monoterpenes with O3. *Environ. Sci. Technol.* **2005**, *39* (11), 4049−4059.
(51) Berkemeier, T.; Ammann, M.; Krieger, U. K.; Peter, T.; Spichtinger, P.; Pöschl, U.; Shiraiwa, M.; Huisman, A. J. Monte Carlo genetic algorithm (MCGA) for model analysis of multiphase chemical kinetics to determine transport and reaction rate coefficients using multiple experimental data sets. *Atmos. Chem. Phys.* **2017**, *17* (12), 8021−8029.
(52) Robertson, D. E.; Prince, R. C.; Bowyer, J. R.; Matsuura, K.; Dutton, P. L.; Ohnishi, T. Thermodynamic properties of the semiquinone and its binding site in the ubiquinol-cytochrome c (c2) oxidoreductase of respiratory and photosynthetic systems. *J. Biol. Chem.* **1984**, *259* (3), 1758−1763.

DOI: 10.1021/acs.est.8b03695
Environ. Sci. Technol. 2018, 52, 11642−11651

(53) Vejerano, E.; Lomnicki, S. M.; Dellinger, B. Formation and stabilization of combustion-generated, environmentally persistent radicals on Ni (II) O supported on a silica surface. *Environ. Sci. Technol.* **2012**, *46* (17), 9406−9411.
(54) Kiruri, L. W.; Khachatryan, L.; Dellinger, B.; Lomnicki, S. Effect of copper oxide concentration on the formation and persistency of environmentally persistent free radicals (EPFRs) in particulates. *Environ. Sci. Technol.* **2014**, *48* (4), 2212−2217.
(55) Surratt, J. D.; Murphy, S. M.; Kroll, J. H.; Ng, N. L.; Hildebrandt, L.; Sorooshian, A.; Szmigielski, R.; Vermeylen, R.; Maenhaut, W.; Claeys, M.; Flagan, R. C.; Seinfeld, J. H. Chemical composition of secondary organic aerosol formed from the photooxidation of isoprene. *J. Phys. Chem. A* **2006**, *110* (31), 9665−9690.
(56) Kautzman, K. E.; Surratt, J. D.; Chan, M. N.; Chan, A. W. H.; Hersey, S. P.; Chhabra, P. S.; Dalleska, N. F.; Wennberg, P. O.; Flagan, R. C.; Seinfeld, J. H. Chemical composition of gas-and aerosol-phase products from the photooxidation of naphthalene. *J. Phys. Chem. A* **2010**, *114* (2), 913−934.
(57) Wendlandt, A. E.; Stahl, S. S. Quinone-Catalyzed Selective Oxidation of Organic Molecules. *Angew. Chem., Int. Ed.* **2015**, *54* (49), 14638−14658.
(58) Chen, X.; Hopke, P. K.; Carter, W. P. L. Secondary organic aerosol from ozonolysis of biogenic volatile organic compounds: chamber studies of particle and reactive oxygen species formation. *Environ. Sci. Technol.* **2011**, *45* (1), 276−282.
(59) Wang, Y.; Arellanes, C.; Paulson, S. E. Hydrogen peroxide associated with ambient fine-mode, diesel, and biodiesel aerosol particles in Southern California. *Aerosol Sci. Technol.* **2012**, *46* (4), 394−402.
(60) Arellanes, C.; Paulson, S. E.; Fine, P. M.; Sioutas, C. Exceeding of Henry's law by hydrogen peroxide associated with urban aerosols. *Environ. Sci. Technol.* **2006**, *40* (16), 4859−4866.
(61) Charrier, J. G.; McFall, A. S.; Richards-Henderson, N. K.; Anastasio, C. Hydrogen peroxide formation in a surrogate lung fluid by transition metals and quinones present in particulate matter. *Environ. Sci. Technol.* **2014**, *48* (12), 7010−7.
(62) Buettner, G. R. The pecking order of free radicals and antioxidants: lipid peroxidation, α-tocopherol, and ascorbate. *Arch. Biochem. Biophys.* **1993**, *300* (2), 535−543.
(63) Pryor, W. A.; Church, D. F. Aldehydes, hydrogen peroxide, and organic radicals as mediators of ozone toxicity. *Free Radical Biol. Med.* **1991**, *11* (1), 41−46.
(64) Li, H.; Chen, Z.; Huang, L.; Huang, D. Organic peroxides' gas-particle partitioning and rapid heterogeneous decomposition on secondary organic aerosol. *Atmos. Chem. Phys.* **2016**, *16* (3), 1837−1848.
(65) Chevallier, E.; Jolibois, R. D.; Meunier, N.; Carlier, P.; Monod, A. Fenton-like" reactions of methylhydroperoxide and ethylhydroperoxide with Fe 2+ in liquid aerosols under tropospheric conditions. *Atmos. Environ.* **2004**, *38* (6), 921−933.
(66) Nam, W.; Han, H. J.; Oh, S.-Y.; Lee, Y. J.; Choi, M.-H.; Han, S.-Y.; Kim, C.; Woo, S. K.; Shin, W. New Insights into the mechanisms of O− O bond cleavage of hydrogen peroxide and tert-alkyl hydroperoxides by iron (III) porphyrin complexes. *J. Am. Chem. Soc.* **2000**, *122* (36), 8677−8684.
(67) McWhinney, R. D.; Zhou, S.; Abbatt, J. Naphthalene SOA: redox activity and naphthoquinone gas−particle partitioning. *Atmos. Chem. Phys.* **2013**, *13* (19), 9731−9744.
(68) Guin, P. S.; Das, S.; Mandal, P. C. Electrochemical Reduction of Quinones in Different Media: A Review. *Int. J. Electrochem.* **2011**, *2011*, 1−22.
(69) Jones, C. M.; Lawrence, A.; Wardman, P.; Burkitt, M. J. Electron paramagnetic resonance spin trapping investigation into the kinetics of glutathione oxidation by the superoxide radical: re-evaluation of the rate constant. *Free Radical Biol. Med.* **2002**, *32* (10), 982−990.
(70) Verma, V.; Fang, T.; Xu, L.; Peltier, R. E.; Russell, A. G.; Ng, N. L.; Weber, R. J. Organic aerosols associated with the generation of reactive oxygen species (ROS) by water-soluble PM2.5. *Environ. Sci. Technol.* **2015**, *49* (7), 4646−56.
(71) Xiong, Q.; Yu, H.; Wang, R.; Wei, J.; Verma, V. Rethinking Dithiothreitol-Based Particulate Matter Oxidative Potential: Measuring Dithiothreitol Consumption versus Reactive Oxygen Species Generation. *Environ. Sci. Technol.* **2017**, *51* (11), 6507−6514.
(72) Tuet, W. Y.; Chen, Y.; Fok, S.; Champion, J. A.; Ng, N. L. Inflammatory responses to secondary organic aerosols (SOA) generated from biogenic and anthropogenic precursors. *Atmos. Chem. Phys.* **2017**, *17* (18), 11423−11440.
(73) Chowdhury, P. H.; He, Q.; Lasitza Male, T.; Brune, W. H.; Rudich, Y.; Pardo, M. Exposure of Lung Epithelial Cells to Photochemically Aged Secondary Organic Aerosol Shows Increased Toxic Effects. *Environ. Sci. Technol. Lett.* **2018**, *5* (7), 424−430.
(74) Arashiro, M.; Lin, Y.-H.; Zhang, Z.; Sexton, K. G.; Gold, A.; Jaspers, I.; Fry, R. C.; Surratt, J. D. Effect of secondary organic aerosol from isoprene-derived hydroxyhydroperoxides on the expression of oxidative stress response genes in human bronchial epithelial cells. *Environ. Sci.: Processes Impacts* **2018**, *20*, 332−339.
(75) Soyer, O. U.; Dizdar, E. A.; Keskin, O.; Lilly, C.; Kalayci, O. Comparison of two methods for exhaled breath condensate collection. *Allergy* **2006**, *61* (8), 1016−1018.
(76) Haugen, T. S.; Skjonsberg, O. H.; Kahler, H.; Lyberg, T. Production of oxidants in alveolar macrophages and blood leukocytes. *Eur. Respir. J.* **1999**, *14* (5), 1100−1105.
(77) Kietzmann, D.; Kahl, R.; Müller, M.; Burchardi, H.; Kettler, D. Hydrogen peroxide in expired breath condensate of patients with acute respiratory failure and with ARDS. *Intensive Care Med.* **1993**, *19* (2), 78−81.
(78) Emelyanov, A.; Fedoseev, G.; Abulimity, A.; Rudinski, K.; Fedoulov, A.; Karabanov, A.; Barnes, P. J. Elevated concentrations of exhaled hydrogen peroxide in asthmatic patients. *Chest* **2001**, *120* (4), 1136−1139.
(79) Van Beurden, W. J. C.; Dekhuijzen, P. N. R.; Harff, G. A.; Smeenk, F. W. J. M. Variability of exhaled hydrogen peroxide in stable COPD patients and matched healthy controls. *Respiration* **2002**, *69* (3), 211−216.
(80) Nagaraja, C.; Shashibhushan, B. L.; Sagar, M. A.; Manjunath, P. H.; Asif, M. Hydrogen peroxide in exhaled breath condensate: A clinical study. *Lung India* **2012**, *29* (2), 123−127.
(81) Kharitonov, S. A.; Barnes, P. J. Exhaled markers of pulmonary disease. *Am. J. Respir. Crit. Care Med.* **2001**, *163* (7), 1693−1722.
(82) Schleiss, M. B.; Holz, O.; Behnke, M.; Richter, K.; Magnussen, H.; Jorres, R. A. The concentration of hydrogen peroxide in exhaled air depends on expiratory flow rate. *Eur. Respir. J.* **2000**, *16* (6), 1115−1118.

DOI: 10.1021/acs.est.8b03695
Environ. Sci. Technol. 2018, 52, 11642−11651